One Element Per Grain: An Effcient Virtual Element Method for Heat Conduction in Polycrystalline Materials

Sundararajan Natarajan*

Department of Mechanical Engineering, Indian Institute of Technology Madras, Chennai - 600036, Tamil Nadu, India

Abtract: An efficient numerical framework based on the virtual element method is proposed to study the heat conduction in polycrystalline materials. Voronoi tessellation is used to generate a representative micro-structure, with grain boundaries explicitly modelled in two dimensions. The proposed framework treats each grain/grain boundary as one finite element and this feature drastically reduces the computational time. The numerical results from the proposed framework are compared with traditional finite element, where each grain/grain boundary is discretized with simplex elements. The numerical assessment demonstrates the effectiveness and robustness of the framework and yield accurate results at a fraction of computational effort without compromising accuracy. From the numerical study, it is observed that the proposed framework requires *at least an order* of magnitude fewer dofs when compared to the FEM.

Keywords: Effective thermal conductivity, Grain boundary, Grain core, Polycrystalline material, Polygon, Virtual element method.

1. INTRODUCTION

Grains and grain boundaries of a polycrystalline material govern its macroscopic responses [1]. For instance, the mechanical response of an alloy in many ways depends on the size of grains [2] and the properties of its grain boundaries [3]. Other examples include the role of grain sizes and grain boundaries in affecting the electrical [4] or thermal conductivity of polycrystalline materials [5]. Clearly, establishing a relation between the nature of grains and the grain boundaries of a polycrystalline sample and its properties is extremely important.

Traditionally, the finite element method (FEM) has been used to estimate the temperature distribution and effective thermal conductivity of a polycrystalline sample. The FEM requires spatial dicretization of a computational domain with non-overlapping elements. Typically, the FEM is restricted to simplex elements, thus, polycrystalline samples have to be further discretized to compute the temperature distribution and other quantities of interest. The domain of interest when estimating the effective properties is a microstructure that consists of grains and grain boundaries. To employ the FEM, the region is discretized with simplex elements, this inherently restricts the number of grains and the size of the microstructure to be analyzed. Similarly, in [6, 7], the boundary element method (BEM) is used to study the polycrystalline materials. The morphology is represented through Voronoi tessellations, but to apply BEM, a quality triangular/quadrangular boundary elements are generated on each individual grains (or Voronoi cell).

To alleviate the meshing restrictions imposed by traditional FEM, research has focussed on developing numerical framework that accommodates elements with arbitrary shapes and sizes. Some of the popular approaches include, the polygonal finite element method [8], the scaled boundary finite element method and the virtual element method [9-12]. All aforementioned approaches are seen as a generalization of the FEM. Amongst these, the VEM, unlike FEM, does not require an explicit form for the basis functions to compute the bilinear and linear form within the Galerkin framework, which makes this framework computationally less intensive and distortion insensitive. The accuracy and the stability of the method is ensured by assuming polynomials and additional functions over each element [10-13]. The flexibility and the robustness that the VEM offers, has attracted researchers to apply it to a wide variety of problems in engineering and science, see for example, [14-22] and references therein. In [23], the performance of VEM is studied for 2D elastostatics problem over the homogenized polycrystalline materials and unidirectional fibre-reinforced composites.

The main objective of this work is to use the virtual element method (VEM) and treat each grain and grain boundary as a single element, consequently reducing the number of degrees of freedom and hence the computational cost. Consequently, the domain of interest in this work is a microstructure, with explicit

*Address correspondence to this author at Department of Mechanical Engineering, Indian Institute of Technology Madras, Chennai - 600036, Tamil Nadu, India; E-mail: snatarajan@iitm.ac.in

E-ISSN: 3110-9780/25

grain boundary regions so that properties can be specified to it. There are several codes/softwares which can generate microstructures with various levels of sophistication and options. In particular *MicroStructPy* [24], a easy-to-use python based code has been used recently to understand multiparticle interactions in composite electrodes [25] and the role of finite sized specimens [26]. Another, commonly used code is *Neper* [27, 28] produces statistically representative microstructures and has been used extensively. *Neper2CAE* and *PyCiGen* [29] are two other codes which can generate cohesive elements in between grains for the commercial finite element code, ABAQUS.

In all of aforementioned codes, the grains can be modelled with significant level of detail, but they do not allow explicitly modelling the grain boundary or control some of its properties. It would also be convenient to read the generated microstructure geometry by open source software GMSH [30]. The geometry can then be discretized with appropriate elements for finite element analysis. It is also necessary that relevant entities of the geometry be tagged so that material properties and boundary conditions can be applied. In this work a small package is built on top of *MicroStructPy* to generate microstructures, with explicit grain boundary domains, the details of which are presented in Section 4.

We propose to employ the virtual element method (VEM) framework for spatial discretization of the microstructure where each grain/grain boundary region is represented as *one* single element. The objectives of the present work is are as follows:

- Compute the effective thermal conductivity of polycrystalline materials with explicit modeling of grain boundaries in two dimensions.
- To improve the accuracy of the solution, higher order VEM is explored.
- Extend the framework to three dimensions and study heat conduction in a typical polycrystalline material.

The rest of the paper is organized as follows: Section 2 presents the governing differential equation for heat diffusion in polycrystalline materials. An overview of the virtual element method and its application to the heat diffusion equation is presented in Section 3. The generation of polycrystalline microstructure with explicit representation of the grain boundaries and triple junctions is presented in Section 4. The effective thermal conductivity, steady state and transient heat response in 2 and 3 dimensions of a representative polycrystalline material is numerically computed using the proposed framework in Section 5, followed by conclusions in the last section.

2. THEORETICAL FORMULATION

Consider a evolution problem on a homogeneous anisotropic body occupying an open domain $\Omega \subset \mathbb{R}^d, d = 2,3$ with a closure $\overline{\Omega}$. The external boundary is defined by $\Gamma = \overline{\Omega} / \Omega$ accommodates the following decompositions: $\Gamma = \Gamma_1 \cup \Gamma_2$ and $\Gamma_1 \cap \Gamma_2 = \varnothing$, where Dirichlet and Neumann boundary conditions are applied on Γ_1 and Γ_2 , respectively. The following parabolic problem is considered: find $\theta \in C(0,T,C^2(\Omega)),$ such that:

$$-\nabla \cdot \left(\kappa \nabla \theta(\mathbf{x},t)\right) + Q(\mathbf{x},t) = \rho C_p \dot{\theta}, \qquad in \qquad \Omega \times (0,T], \tag{1}$$

where $\theta(\mathbf{x})$ is the temperature field, $\kappa = \begin{bmatrix} k_{xx} & k_{xy} \\ k_{yx} & k_{yy} \end{bmatrix}$ represents the thermal conductivity matrix, ρ and C_p are the density and the specific heat at constant pressure, respectively, $\nabla = \left\{ \frac{\partial}{\partial x}, \frac{\partial}{\partial y} \right\}^\tau$ for two dimensions and $\nabla = \left\{ \frac{\partial}{\partial x}, \frac{\partial}{\partial y}, \frac{\partial}{\partial z} \right\}^T$ for three dimensions, is the scalar Laplacian operator, $\dot{\theta}$ denotes the time derivative of the temperature field and $Q(\mathbf{x},t)$ is the heat source. EQ5 is supplemented with the following boundary conditions:

$$\theta(\mathbf{x},t) = \overline{\theta}(\mathbf{x}), \qquad on \quad \Gamma_1 \times [0,T] \tag{2a}$$

$$\mathbf{q}(\mathbf{x},t) = \overline{\mathbf{q}}(\mathbf{x}), \qquad on \quad \Gamma_2 \times [0,T] \tag{2b}$$

where $\mathbf{q}(\mathbf{x},t) = -\kappa \nabla \theta(\mathbf{x},t)$ is the heat flux, $\overline{\theta}$ and $\overline{\mathbf{q}}$ are the applied temperature and heat flux on the boundary. In this work, a representative microstructure including explicit modeling of the grain boundary is done by using Voronoi tessellation. Then, each grain/grain boundary is treated as ' *one*' element for further analysis within the framework of the virtual element method, discussed next.

3. OVERVIEW OF THE VIRTUAL ELEMENT METHOD

We begin by providing the assumptions and properties of the polygonal meshes. Then, we

introduce the VEM spaces followed by a computable VEM formulation.

3.1. Meshes

Let $\{T_h\}_{h>0}$ be a family of polygonal decompositions of the domain Ω. We represent the elements by E and denote the maximum diameter over the polygons by h. Each element $E \in T_h$ satisfies the following assumptions (see [9]),

- E is star-shaped with respect to a disc D_γ of radius γh_E, where h_E is the element diameter,
- for edge $e \subset E$, the length $|e| \geq c h_E$,
- boundary of E is made up of a finite number of edges, where γ and c are positive constants independent of h and E.

Let $P_k(E)$ denote the space of polynomials of degree less than or equal to k on E.

3.2. VEM Spaces

We also recall the definition of projection operators (see [11]) Π_k^∇ and Π_k^0. The projection operator $\Pi_k^\nabla : H^1(E) \to P_k(E)$ is such that,

$$\begin{aligned} &\left(\nabla(w - \Pi_k^\nabla w), \nabla \chi_k\right)_E = \\ &0 \quad \forall \chi_k \in \chi_k(E) \; and \int_{\partial E} (\Pi_k^\nabla w - w) ds = 0, \end{aligned} \tag{3}$$

and the operator Π_k^0 is the L^2 projection onto $P_k(E)$ satisfying,

$$\left(w - \Pi_k^0 w, \chi_k\right)_E = 0 \quad \forall \chi_k \in P_k(E). \tag{4}$$

In a similar way, the polynomial $\Pi_{k-1}^0(\nabla w) \in (P_{k-1}(E))^2$ is computed accomplishing,

$$\left(\nabla w - \Pi_{k-1}^0 \nabla w, \chi_{k-1}\right)_E = 0 \quad \forall \chi_{k-1} \in (P_{k-1}(E))^2. \tag{5}$$

Consider the auxiliary space $V_{E,k}$ (see [31]) for each $E \in T_h$ by,

$$V_{E,k} = \begin{Bmatrix} v \in H^1(E) \cap C^0(\partial E): \\ v_{|e} \in P_k(e) \forall edge e \in \partial E, \Delta v \in P_k(E) \end{Bmatrix}. \tag{6}$$

Now, we define the local virtual element space V_E^k as follows,

$$V_E^k = \begin{Bmatrix} v \in V_{E,k} : \left(v - \Pi_k^\nabla v, \chi\right)_E = \\ 0 \quad \forall \chi \in \left(P_k(E) / P_{k-2}(E)\right) \end{Bmatrix}, \tag{7}$$

where $\left(P_k(E) / P_{k-2}(E)\right)$ is the subset of $P_k(E)$ containing polynomials of degree exactly equal to $k-1$ and k (see [11]). On the space V_E^k, we consider the following set of degrees of freedom (dof):

(G_1) the values of v at the $n(E)$ vertices of polygon E,

(G_2) the values of v at $k-1$ internal Gauss-Lobatto quadrature nodes of every edge $e \in \partial E$,

(G_3) the moments up to order $k-2$ of v in E, i.e.,

$$\int_E v \chi_{k-2} dx \quad \forall \chi_{k-2} \in P_{k-2}(E).$$

We note that the dof mentioned above determines v uniquely on the polygon E, (see [31]). Now, the global virtual element space V_h^k is,

$$V_h^k = \{v \in H_0^1(\Omega) : v_{|E} \in V_E^k \quad \forall E \in T_h\}. \tag{8}$$

3.3 Fully Discrete Virtual Element Formulation

Consider a partition of $(0,T)$ into N disjoint intervals of width $\delta t (= T/N)$ and denote $t_n = n\delta t, n = 0,1,...,N$. Let us denote by θ_h^n, the function θ_h associated to time t_n, i.e. $\theta_h^n := \theta_h(t_n) \in V_h^k$. We use backward Euler method to discretize the time derivative term in the model equation, and virtual element method for spatial discretization. The explicit definition for the basis of virtual element space V_h^k is not known. Hence we use the polynomial projection operators Π_k^∇ and Π_k^0 in defining the linear and bilinear forms of the discrete operator. A computable discrete scheme is formulated as: For $n = 1,2,...,N$, $\forall v_h \in V_h^k$, find $\theta_h^n \in V_h^k$ such that

$$\begin{aligned} &\sum_{E \in T_h} \{\left(\kappa \nabla \Pi_k^\nabla \theta_h^n, \nabla \Pi_k^\nabla v_h\right)_E + \\ &\kappa S_1^E((I - \Pi_k^\nabla)\theta_h^n, (I - \Pi_k^\nabla)v_h) + \left(Q, \Pi_k^0 v_h\right)_E\} = \\ &\sum_{E \in T_h} \{(\rho C_p \frac{\Pi_k^0 \theta_h^{n+1} - \Pi_k^0 \theta_h^n}{\delta t}, \Pi_k^0 v_h)_E + \\ &\rho C_p \, S_2^E((I - \Pi_k^0)\frac{\theta_h^{n+1} - \theta_h^n}{\delta t}, (I - \Pi_k^0)v_h)\}. \end{aligned} \tag{9}$$

In (10), the term S_i^E, i=1,2, are symmetric bilinear forms defined on $V_E^k \times V_E^k$ which ensures that there exists non-zero positive constants μ_*, μ^*, with $\mu_* \leq \mu^*$, independent of h_E, such that $w1.o.g$,

$$\mu_*(\nabla u_h,\nabla u_h)_E \le S_1^E(u_h,u_h) \le \mu^*(\nabla u_h,\nabla u_h)_E$$
$$\forall u_h \in ker(\Pi_k^{\nabla}).$$

$$\mu_*(u_h,u_h)_E \le S_2^E(u_h,u_h) \le \mu^*(u_h,u_h)_E \quad \forall u_h \in ker(\Pi_k^0). \tag{10}$$

In the numerical implementation, a *computable* choice for $S_1^E(\cdot,\cdot)$ and $S_2^E(\cdot,\cdot)$, defined only using the degrees of freedom are given as,

$$S_1^E(u_h,v_h) = \sum_{i=1}^{ndof} dof_i(u_h)dof_i(v_h) \quad and$$
$$S_2^E(u_h,v_h) = |E| \sum_{i=1}^{ndof} dof_i(u_h)dof_i(v_h). \tag{11}$$

where ndof is the total number of degrees of freedom. The terms $S_1^E(\cdot,\cdot)$ and $S_2^E(\cdot,\cdot)$ are referred to as the stabilization terms in the VEM literature and the remaining two terms are known as the consistency terms. The polynomial part of the solution is captured by the consistency term and the stabilization terms captures the non-polynomial part. Interested readers can refer to [9] and references therein.

4. GENERATION OF POLYGONAL MICROSTRUCTURE

The proposed workflow generates an explicit representation of grain boundaries with prescribed width starting from a polycrystalline tessellation. With this workflow, an explicit grain/grain boundary representation is achieved. Given the target number of grains and the desired grain boundary width as inputs, an initial grain structure is generated using the microstruct Python package. Grain edges that are fully contained within the domain are duplicated to enable independent manipulation of adjacent grains, and the element connectivity is updated accordingly. For grains entirely inside the domain, boundary edges are displaced radially inward toward the grain centroid by half of the specified grain boundary width, thereby creating a uniform intergranular gap. For grains intersecting the domain boundary, vertices located on the external boundary are constrained to move along the corresponding grain edges to preserve the domain geometry. The resulting gaps between neighboring grains are explicitly meshed: quadrilateral (four-noded) elements are used along grain edges, while triangular (three-noded) elements are introduced at triple junctions. Geometric operations such as edge offsetting, vertex displacement, and polygon manipulation are performed using the shapely library, enabling robust handling of grain movement and the construction of new grain boundary regions. Algorithm 2 presents the algorithm to generate polycrystalline domain with explicit representation of grain boundaries.

Algorithm 1 Explicit grain boundary construction with prescribed grain boundary width

Require: Number of grains N_g, grain boundary width w_{gb}

Ensure: Polycrystalline mesh with explicit grain boundary regions

1: Generate initial polycrystalline tessellation with N_g grains using microstruct

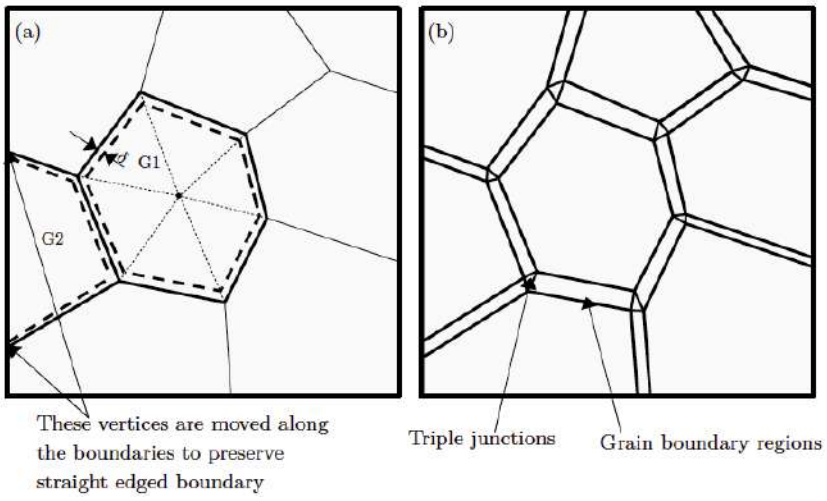

Figure 1: Vertices which are within the domain are pulled towards the centroid of the grain by $\delta = \frac{gbw}{2}$ as in grain G1, while those vertices which are at the domain boundary are moved along the boundary as in shown for the two vertices of grain G2.

2: Identify all grain edges and classify them as internal or boundary edges

3: **for all** internal grain edges **do**

4: Duplicate the edge

5: Update element connectivity so that adjacent grains own separate edges

6: **end for**

7: **for all** grains completely inside the domain **do**

8: Compute grain centroid $\mathbf{c}$

9: **for all** vertices $\mathbf{v}$ on the grain boundary **do**

10: Compute radial direction $\mathbf{d} = \mathbf{v} - \mathbf{c}$

11: Normalize $\mathbf{d}$

12: Move vertex: $\mathbf{v} \leftarrow \mathbf{v} - \frac{w_{gb}}{2}\mathbf{d}$

13: **end for**

14: **end for**

15: **for all** grains intersecting the domain boundary **do**

16: **for all** boundary vertices **do**

17: Constrain vertex motion along the corresponding grain edge

18: **end for**

19: **end for**

20: Identify gaps formed between displaced neighboring grains

21: **for all** gaps along grain edges **do**

22: Mesh gap using four-noded (quadrilateral) elements

23: **end for**

24: **for all** gaps at triple junctions **do**

25: Mesh gap using three-noded (triangular) elements

26: **end for**

27: Perform all geometric operations using shapely

28: Assemble grain interiors and grain boundary elements into final mesh

5. NUMERICAL EXAMPLES

In this section, the VEM framework is employed to study:

- Effective thermal conductivity in two dimensional polycrystalline sample with explicit modelling of grain boundaries.
- Transient heat conduction in two dimensional polycryalline sample.
- Extend the framework to study heat conduction in three dimensional polycrystalline sample.

Each grain and grain boundary (in 2d) of the polycrystalline material is treated as one 'single' element, unlike the traditional FEM, where the grain and the grain boundary needs to be further discretized. The representative micro-structure with explicit modeling of grain boundaries is done using the procedure discussed in pmicrogen in case of two dimensions. For generating three dimensional polycrystalline sample, we use the open-source software Neper [32]. The VEM framework allows easy extension to higher order elements and hence, the order of the polynomial on each element is varied to study the influence on the effective thermal conductivity. The numerical solution of EQ5 for a prescribed boundary condition gives the temperature distribution within the computational domain. The effective thermal conductivity along the $x-$ and the $y-$ direction can be estimated as [33]:

$$\kappa_x^e = \frac{q_x}{\Delta T}\ell\,|_{0\le\ell\le L_x}, \qquad \kappa_y^e = \frac{q_y}{\Delta T}\ell\,|_{0\le\ell\le L_y}, \tag{12}$$

where the q_x is the flux from the left to the right side of the domain and ΔT is the difference in the temperature across the length, L_x and L_y in $x-$ and $y-$ directions, respectively. We note that $\mathbf{q}(\mathbf{x},t) = -\kappa\nabla\theta(\mathbf{x},t)$. The heat fluxes q_x and q_y are the first and second components, respectively, of the vector $\mathbf{q}(\mathbf{x},t)$. Additionally, we remark that, since the basis functions are not known explicitly, the term $\nabla\theta$ is approximated with the help of polynomial projection operator as $\nabla\Pi_k^\nabla\theta$.

For the numerical study, we consider a representative domain of length $L_x = L_y =$ 200 mm containing 21 grains, see Figure **2b**. The grain and the grain boundary is assumed to be homogeneous and isotropic ($\kappa_x = \kappa_y$) and $\kappa_{xy} =$ 0. Further, the thermal

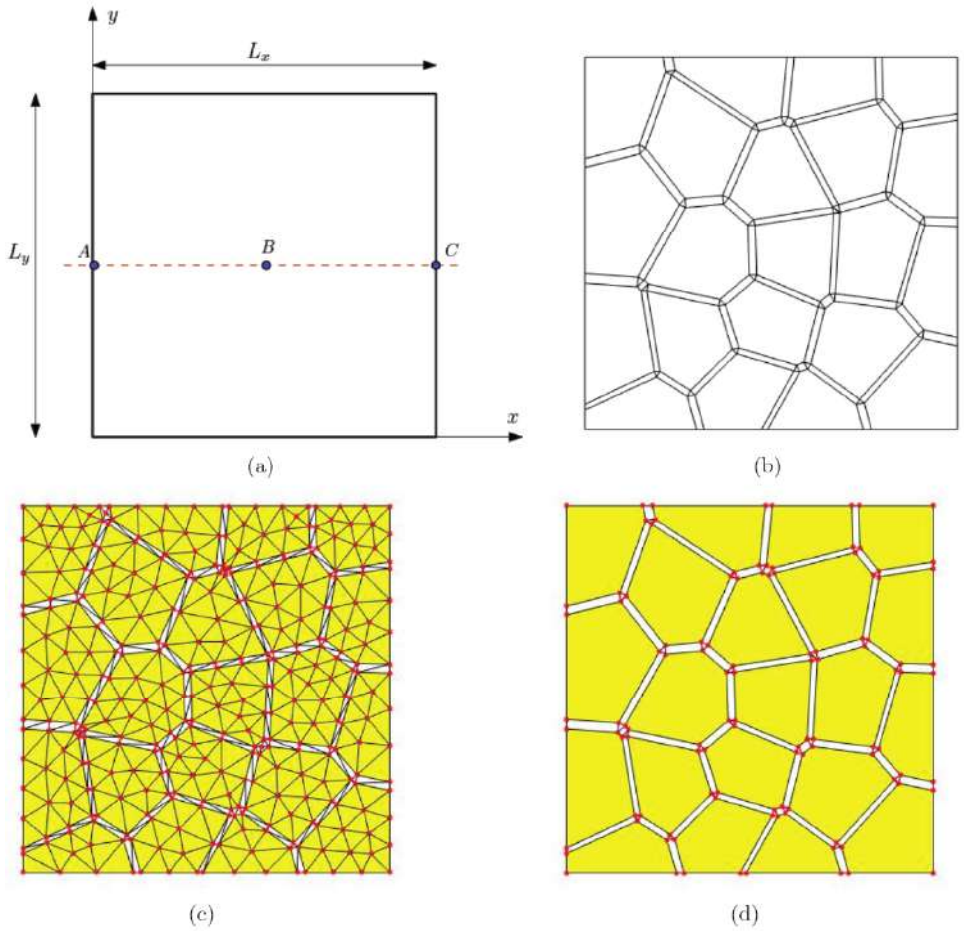

Figure 2: Representative volume element: (**a**) geometry, (**b**) a polycrystalline realization, (**c**) schematic FE mesh and (**d**) virtual element discretization. Note that the grain and grain boundary are represented by 'yellow' and 'white' patch, respectively. The 'red' dots represent the nodes.

conductivity is assumed to be $\kappa_g =$ 10 W/mK for the grain and $\kappa_{gb} =$ 0.1 W/mK for the grain boundary. For estimating the effective thermal conductivity κ_x^e along the $x-$direction, following boundary conditions are used:

$$\theta(0,y)=100K, \quad \theta(L_x,y)=20K, \\ q\cdot\mathbf{n}|_{(x,0)}=0, \quad q\cdot\mathbf{n}|_{(x,L_y)}=0. \tag{13}$$

Similarly, the following conditions

$$\theta(x,0)=100K, \quad \theta(x,L_y)=20K, \\ q\cdot\mathbf{n}|_{(0,y)}=0, \quad q\cdot\mathbf{n}|_{(L_x,y)}=0, \tag{14}$$

are used to compute the effective thermal conductivity, κ_y^e in the $y-$direction. In case of the FEM, each grain/grain boundary is divided into triangles, whilst they are treated as 'one' element within the virtual element framework. Figures **2c** and **2d** show a schematic of finite element and virtual element discretization, respectively. The 'white' region represents the grain boundary and the 'yellow' region represents the grain. To study the convergence properties, $h-$ refinement is adopted in case of the FEM, whilst $k-$refinement is done in case of the VEM. The objective for adopting a $k-$refinement is two folds: (a) to retain the feature of treating each grain/grain boundary as one element and (b) to demonstrate the flexibility, the VEM offers to improve the accuracy. Table **1** shows the effective thermal conductivity κ^e for both the cases.

From Table **1**, it is seen that, $\approx$ 3300 dofs is required to yield an accurate κ^e in case of the FEM, whilst only 417 is required in case of VEM with $k=$ 2, to yield a similar accuracy. The proposed framework requires at least an order of magnitude fewer dofs when compared to the FEM. Similar, results are obtained for the effective thermal conductivity in the $y-$direction, see Table **1**.

Next, to show the robustness of the proposed framework and highlight the computational savings possible a transient heat conduction is solved for the

Table 1: Effective Thermal Conductivity for a Sample with 21 Grains. Note that in Case of VEM, $p-$ Refinement is Adopted, while Treating the Grain/Grain Boundary as One Element.

	h	dofs	κ_x^e	κ_y^e
3*FEM	27.36	339	1.3185	1.3521
	15.33	871	1.3158	1.3554
	0.076	3384	1.3059	1.3415
	0.0398	12026	1.2966	1.3349
	k	dofs	κ_x^e	κ_y^e
3*VEM	1	112	1.2964	1.2813
	2	417	1.2888	1.2788
	3	819	1.2973	1.3302

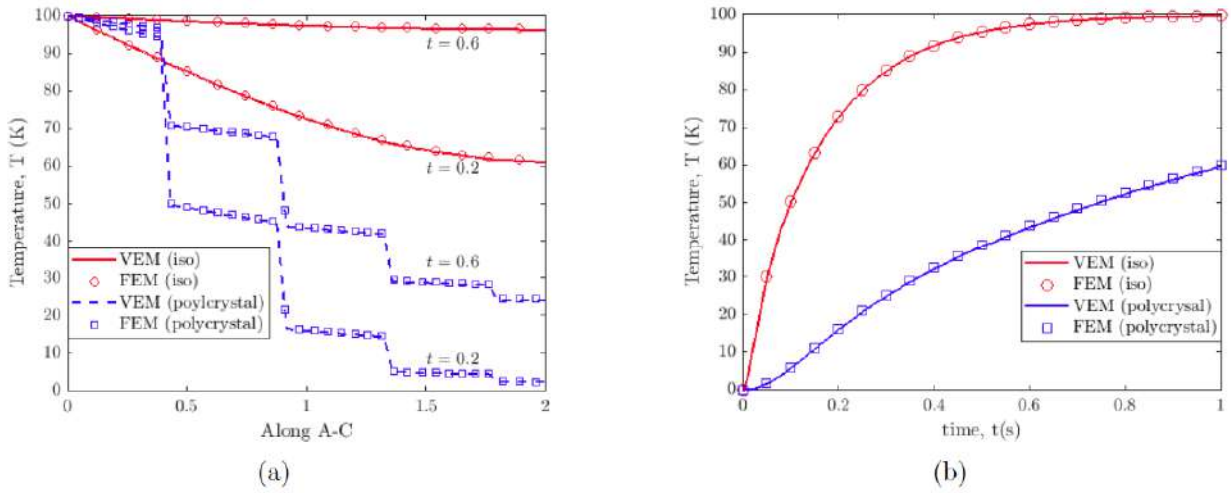

Figure 3: Transient heat conduction: (**a**) temperature distribution along $A-C$ and (**b**) temperature evolution at point B (c.f. Figure **2a**)

same geometry as before. The initial and boundary conditions are taken as: $T(x,y,0)=0,\ \ \theta\ (0,y,t)=100$. On the top and bottom surfaces, zero Neumann conditions are enforced. In case of the FEM, the mesh with 3384 dofs is used while VEM uses $k=$ 2 (417 dofs). For the numerical study, $\Delta\ \theta\ =$ 0.001 is used for both the FEM and the VEM, the simulation is conducted until $\theta=1$. Two cases are studied: (a) both grain and grain boundary have same thermal conductivity, i.e., $\kappa_g=\kappa_{gb}=$ 10 W/mK and (b) thermal conductivity of grain is greater than the grain boundary, i.e., $\kappa_g=$ 10 W/mK and $\kappa_{gb}=$ 0.1 W/mK. For numerical calculations, ρC_p is taken as 1. Figure **3a** shows the temperature distribution along $A-C$ (c.f. Figure **2a**) at different time instances for both the cases. The discontinuity seen is attributed to the different thermal conductivity of the grain and the grain boundary. The temperature evolution at point B (c.f. Figure **2a**) is shown in Figure **3b**. It is seen that in case of different conductivity of the grain and the grain boundary, the heat conduction is slower as expected. From Figure **3**, it is inferred that the results from the present framework matches closely with that of the finite element solution.

Next, we consider a cube $\Omega=[0,1]^3$ with 12 grains, see Figure **4**. The temperature on the bottom face, ie., $z=$ 0 plane is set at $\theta\ =$ 0 K and the top face ie., $z=$ 1 is subjected to a constant temperature, $\theta\ =$ 100 K. On all other faces, the flux is assumed to be zero, i.e., $q\cdot\mathbf{n}=$ 0. In case of the VEM, similar to the 2d case, each grain is treated as one polyhedral element, whilst, the grain is divided into tetrahedral elements in case of the standard FEM, with a mesh size of 1mm is maintained. Figure **5** shows the temperate along the vectors: (a) $P(0,0,0)\rightarrow Q(1,1,1)$ and (b) $R(1/2,1/2,0)\rightarrow S(1/2,1/2,1)$. The results from the present framework is compared with the traditional FEM and it is inferred that the results are in close agreement. Note that for demonstration, only lower

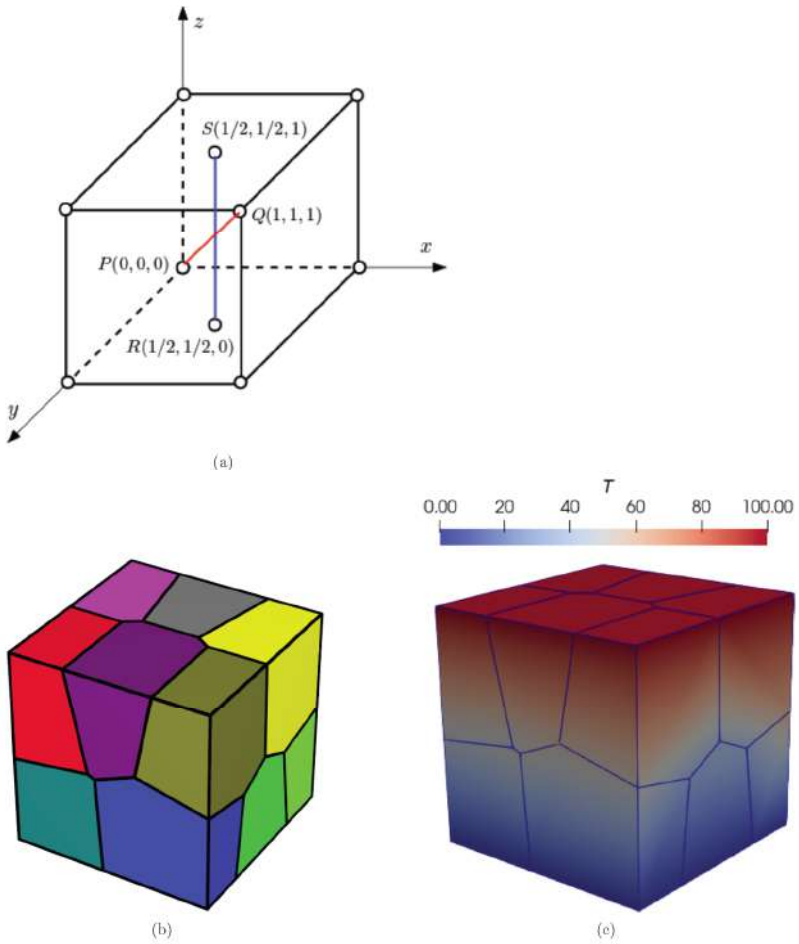

Figure 4: Representative volume element in 3d: (**a**) geometry, (**b**) schematic polycrystalline realization and (**c**) temperature distribution.

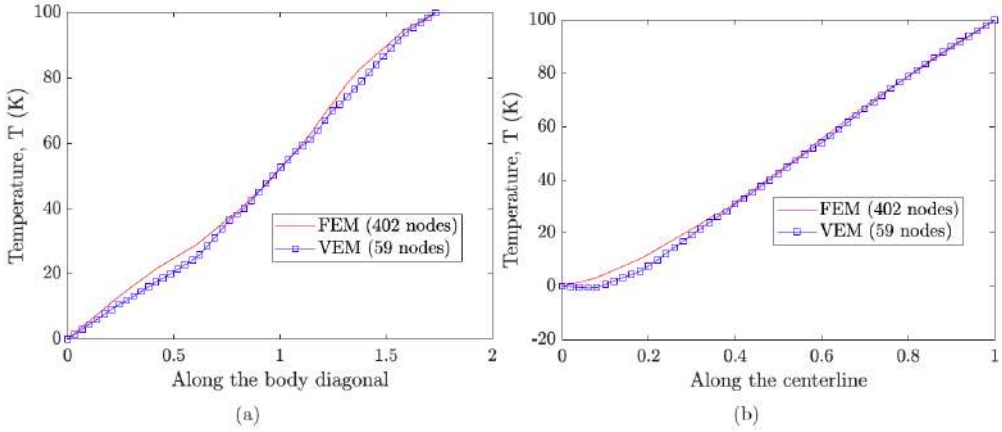

Figure 5: Temperature along the vectors: (**a**) $P(0,0,0) \rightarrow Q(1,1,1)$ and (**b**) $R(1/2,1/2,0) \rightarrow S(1/2,1/2,1)$, comparison with traditional FEM.

order VEM is employed and explicit modelling of the grain boundaries is ignored.

6. CONCLUSIONS

A numerical framework based on the virtual element method is proposed to compute the effective thermal conductivity and the temperature distribution in a polycrystalline materials. The salient feature of the proposed framework is that unlike the traditional finite element method, the grains/grain boundaries need not be spatially discretized with simplex elements. From the numerical study, it can be inferred that the

proposed framework reduces the computational efforts, yields comparable results without compromising on the accuracy. Further, the applicability of the framework for 3D polycrystalline materials is demonstrated. In particular, it requires at least an order of magnitude fewer dofs when compared to the traditional FEM with simplex elements for both 2d and 3d domains. We believe the proposed framework will be very useful when assessing the influence of randonmness in the grain orientation, thermal conductivity and grain size on the global response. The proposed methodology can be employed within the framework for FE^2, which will be a topic of future communication. One potential limitation of the proposed approach arises when each grain is modeled as a single element, particularly in the context of transient diffusion analyses in highly anisotropic polycrysalline samples. In such cases, if the characteristic grain size is larger than the relevant thermal diffusion length scale, the underlying physics associated with intra-grain temperature gradients may not be adequately captured. Therefore, care must be exercised in transient simulations to ensure that the chosen discretization is consistent with the governing physical length and time scales. This can be done either by increasing the polynomial order or by subdividing the grain to minimum number so as to capture the necessary physics.

ACKNOWLEDGEMENTS

The author would like to acknowledge the discussions with Prof. N Swaminathan, IIT Madras and for his code to generate polycrystals based on Voronoi tessellation. Also acknowledge the discussions with Dr. Arrutselvi on the virtual element framework.

REFERENCES

[1] Torquato S. Random Heterogeneous Materials: Microstructure and Macroscopic Properties, Interdisciplinary Applied Mathematics, Springer New York, 2013. URL https://books.google.co.in/books?id=UTfoBwAAQBAJ

[2] Droste M, Jarvenpaa A, Jaskari M, Motylenko M, Weidner A, Karjalainen P, Biermann H. The role of grain size in static and cyclic deformation behaviour of a laser reversion annealed metastable austenitic steel. Fatigue & Fracture of Engineering Materials & Structures 2021; 44(1): 43-62. https://doi.org/10.1111/ffe.13326

[3] Schuh CA, Lu K. Stability of nanocrystalline metals: The role of grain-boundary chemistry and structure. MRS Bulletin 2021; 1-11. https://doi.org/10.1557/s43577-021-00055-x

[4] Symington AR, Molinari M, Dawson JA, Statham JM, Purton J, Canepa P, Parker SC. Elucidating the nature of grain boundary resistance in lithium lan thanum titanate. Journal of Materials Chemistry A 2021; 9(10): 6487-6498. https://doi.org/10.1039/D0TA11539H

[5] Badry F, Ahmed K. A new model for the effective thermal conductivity of poly285 crystalline solids. AIP Advances 2020; 10(10): 105021. https://doi.org/10.1063/5.0022375

[6] Gulizzi V, Milazzo A, Benedetti I. An enhanced grain-boundary framework for computational homogenization and micro-cracking simulations of polycrystalline materials. Computational Mechanics 2015; 56(4): 631-651. https://doi.org/10.1007/s00466-015-1192-8

[7] Cascio ML, Gulizzi V, Milazzo A, Benedetti I. A model for pol-ycrystalline thermo-mechanical homogenisation and micro-cracking. Procedia Structural In tegrity 2024; 52: 618-624. https://doi.org/10.1016/j.prostr.2023.12.063

[8] Manzini G, Russo A, Sukumar N. New perspectives on polygonal and polyhedral finite element methods. Mathematical Models and Methods in Applied Sciences 2014; 24(08): 1665-1699. https://doi.org/10.1142/S0218202514400065

[9] Veiga LBD, Brezzi F, Cangiani A, Manzini G, Marini LD, Russo A. Basic principles of Virtual Element Methods. Math Models Methods Appl Sci 2013; 23: 199-214. https://doi.org/10.1142/S0218202512500492

[10] Veiga LBD, Brezzi F, Marini LD, Russo A. The Hitchikkers Guide to the Virtual Element Method. Math Models Methods Appl Sci 2014; 24: 1541-1574. https://doi.org/10.1142/S021820251440003X

[11] Veiga LBD, Brezzi F, Marini LD, Russo A. Virtual Element Method for general second-order elliptic problems. Math Models Methods Appl Sci 2016; 26(4): 729-750. https://doi.org/10.1142/S0218202516500160

[12] Vacca G, Beirao Da Veiga L. Virtual element methods for parabolic problems on polygonal meshes. Numer Meth Part D E 2015; 31(6): 2110-2134. https://doi.org/10.1002/num.21982

[13] Vacca G. Virtual element methods for hyperbolic problems on polygonal meshes. Comput Math Appl 2017; 74(5): 882-898. https://doi.org/10.1016/j.camwa.2016.04.029

[14] A. Cangiani, G. Manzini, O. J. Sutton, Conforming and nonconforming virtual element methods for elliptic problems. IMA Journal of Numerical Analysis 2017; 37(3): 1317-1354. https://doi.org/10.1093/imanum/drw036

[15] Benedetto MF, Berrone S, Borio A, Pieraccini S, Scialo S. Order preserving supg stabilization for the virtual element formulation of advection-di”usion problems. Comput Methods Appl Mech Eng 2016; 311: 18-40. https://doi.org/10.1016/j.cma.2016.07.043

[16] Adak D, Natarajan E, Kumar S. Convergence analysis of virtual element methods for semilinear parabolic problems on polygonal meshes. Numer Meth Part D E 2019; 35(1): 222-245. https://doi.org/10.1002/num.22298

[17] Adak D, Natarajan E, Kumar S. Virtual element method for semilinear hyper bolic problems on polygonal meshes. Int J Comput Math 2019; 96(5): 971-991. https://doi.org/10.1080/00207160.2018.1475651

[18] Adak D, Natarajan S, Natarajan E. Virtual element method for semilinear elliptic problems on polygonal meshes. Appl Numer Math 2019; 145: 175-187. https://doi.org/10.1016/j.apnum.2019.05.021

[19] Beirao Da Veiga L, Lovadina C, Mora D. A virtual element method for elastic and inelastic problems on polytope meshes, Comput Methods Appl Mech Eng 2015; 295: 327-346. https://doi.org/10.1016/j.cma.2015.07.013

[20] Beirao Da Veiga L, Brezzi F, Marini LD, Virtual elements for linear elasticity problems. SIAM J Numer Anal 2013; 51: 794-812. https://doi.org/10.1137/120874746

[21] Gain AL, Talischi C, Paulino GH. On the virtual element method for three dimensional linear elasticity problems on arbitrary polyhedral meshes. Comput Methods Appl Mech Eng 2014; 282: 132-160. https://doi.org/10.1016/j.cma.2014.05.005

[22] Antonietti PF, Beirao Da Veiga L, Scacchi S, Verani M. A c1 virtual element method for the cahn-hilliard equation with polygonal meshes. SIAM J Numer Anal 2016; 54(1): 34-56. https://doi.org/10.1137/15M1008117

[23] Lo Cascio M, Milazzo A, Benedetti I. Virtual element method for computational homogenization of composite and heterogeneous materials. Composite Structures 2020; 232: 111523. https://doi.org/10.1016/j.compstruct.2019.111523

[24] Hart KA, Rimoli JJ. Microstructpy: A statistical microstructure mesh gener ator in python. SoftwareX 2020; 12: 100595. https://doi.org/10.1016/j.softx.2020.100595

[25] Bistri D, Di Leo CV. Modeling of chemo-mechanical multi-particle interactions in composite electrodes for liquid and solid-state liion batteries. Journal of The Electrochemical Society 2021; 168(3): 030515. https://doi.org/10.1149/1945-7111/abe8ea

[26] Zuanetti B, Luscher DJ, Ramos K, Bolme C. Unraveling the implications of finite specimen size on the interpretation of dynamic experiments for polycrys talline aluminum through direct numerical simulations. International Journal of Plasticity 2021; 103080. https://doi.org/10.1016/j.ijplas.2021.103080

[27] Quey R, Renversade L. Optimal polyhedral description of 3d polycrystals: Method and application to statistical and synchrotron x-ray di”raction data, Computer Methods in Applied Mechanics and Engineering 2018; 330: 308-333. https://doi.org/10.1016/j.cma.2017.10.029

[28] Rimoli J, Ortiz M. A duality-based method for generating geometric representa tions of polycrystals. International Journal for Numerical Methods in Engineering 2011; 86(9): 1069-1081. https://doi.org/10.1002/nme.3090

[29] Grilli N, Tarleton E, Cocks AC. Neper2cae and pycigen: Scripts to generate polycrystals and interface elements in abaqus. SoftwareX 2021; 13: 100651. https://doi.org/10.1016/j.softx.2020.100651

[30] Geuzaine C, Remacle J-F. Gmsh 2009.

[31] Ahmad B, Alsaedi A, Brezzi F, Marini D, Russo LA. Equivalent projectors for virtual element methods. Comput Math with Appl 2013; 66: 376-391. https://doi.org/10.1016/j.camwa.2013.05.015

[32] Quey R, Dawson P, Barbe F. Large-scale 3D random polycrystals for the fi nite element method: Generation, meshing and remeshing. Computer Methods in Applied Mechanics and Engineering 2011; 200: 1729-1745. https://doi.org/10.1016/j.cma.2011.01.002

[33] Saini A, Unnikrishnakurup S, Krishnamurthy C, Balasubramanian K, Sundararajan T. Numerical study using finite element method for heat conduction on heterogeneous materials with varying volume fraction, shape and size of fillers International Journal of Thermal Sciences 2021; 159: 106545. https://doi.org/10.1016/j.ijthermalsci.2020.106545

Received on 20-11-2025 Accepted on 25-12-2025 Published on 31-12-2025

https://doi.org/10.66000/3110-9780.2025.01.08